

Charge-density waves in deconfining SU(2) Yang-Mills thermodynamics

Carlos Falquez*, Ralf Hofmann**, and Tilo Baumbach*

* *Laboratorium für Applikationen der Synchrotronstrahlung (LAS)*
Karlsruher Institut für Technologie (KIT)
Postfach 6980
76128 Karlsruhe, Germany

** *Institut für Theoretische Physik*
Universität Heidelberg
Philosophenweg 16
69120 Heidelberg, Germany

Abstract

At one-loop accuracy we compute, characterize, and discuss the dispersion laws for the three low-momentum branches of propagating longitudinal, electric U(1) fields in the effective theory for the deconfining phase of pure SU(2) Yang-Mills thermodynamics. With an electric-magnetically dual interpretation of $SU(2)_{\text{CMB}}$ we argue that upon a breaking of plasma isotropy and homogeneity, introduced e.g. by a temperature gradient, the longitudinal modes could conspire to provide magnetic seed fields for magneto-hydrodynamical dynamos inside structures of galaxy, galaxy-cluster, and cosmological scales. Such a scenario ultimately links structure with seed-field formation. As judged from the present cosmological epoch, the maximally available coherent field strength of 10^{-8} Gauss from $SU(2)_{\text{CMB}}$ matches with the upper bound for cosmological present-day field strength derived from small-angle anisotropies of the cosmic microwave background.

1 Introduction

In its two phases with propagating gauge fields the thermal ground states of $SU(2)$ Yang-Mills thermodynamics exhibit macroscopic behavior which in some respects resembles that of metals. By a selfconsistent spatial coarse-graining in Euclidean signature over quantum fluctuations of trivial [1, 2] and nontrivial topology [3, 4, 5, 6, 7, 8] precise estimates of the ground-state physics are obtained in both phases [9, 10, 12]. The thermal ground states determine the properties of effective and very weakly or noninteracting thermal quasiparticle excitations [9, 10, 11, 12]. While in the deconfining phase one direction of the three dimensional Lie algebra of $SU(2)$ remains massless ('photon') the only (noninteracting) propagating gauge mode in the pre-confining phase is massive due to the dual Meissner effect and the decoupling of massive modes at the deconfining-preconfining phase boundary. In the deconfining phase nontrivial dispersion laws for the three polarizations states of the massless $U(1)$ gauge mode occur through resummed one-loop radiative corrections. In [13] the dispersion for transversely polarized 'photons' was computed and further characterized in [14]. In the context of $SU(2)_{\text{CMB}}$ [10, 15] this¹ dispersion predicts a gap in the spectrum of black-body radiation at low temperatures and frequencies, see [23] for an investigation of experimental signatures. The dispersion of the longitudinal polarization has not been investigated so far. Longitudinal modes are absent on tree level. Moreover, according to an electric-magnetically dual interpretation of $SU(2)_{\text{CMB}}$ they represent longitudinally propagating, long-wavelength magnetic fields whose intensity can not be measured by a detector.

In the present work we investigate the propagation properties of these longitudinal modes. In deconfining $SU(2)$ Yang-Mills thermodynamics (no electric-magnetically dual interpretation) they are associated with the propagation of radiatively induced, electric charge densities. The computation is performed in analogy to [13], where the propagation of transverse modes was studied, by a one-loop selfconsistent resummation of the longitudinal component of the massless mode's polarization tensor. As a result and in contrast to the transverse case, three branches of longitudinal modes occur at low momenta. Scaling out temperature, their high-temperature dispersion is temperature independent. One branch resembles a finite-support light-like dispersion. Microscopically, such a behavior should be associated with the slow motion of stable magnetic monopoles and antimonopoles released by large-holonomy (anti)calorons upon dissociation [8, 24]. The other branches exhibit superluminal group velocities which suggest their association with instantaneous spatial correlations between short-lived but fast-moving magnetic monopoles and antimonopoles.

¹This postulate states that, fundamentally, the propagation of electromagnetic waves is described by an $SU(2)$ rather than a $U(1)$ gauge principle. Observations of the Cosmic Microwave Background (CMB) then suggest [16, 17] that the critical temperature for the deconfining-preconfining phase transition coincides with the CMB's present temperature [18, 19], hence the term $SU(2)_{\text{CMB}}$. Interplaying with an axion field of Planckian origin [15, 20, 21, 22] the thermal-ground state physics of $SU(2)_{\text{CMB}}$ could be responsible for the (dominant) dark-energy component in today's mix of cosmological fluids.

(Anti)monopoles of this type occur in small-holonomy (anti)calorons [8, 24].

The paper is organized as follows. In Sec. 2 we explain how the temporal component of the polarization tensor of the massless mode is related to the screening function F in the dispersion law and how F is computed selfconsistently at one-loop accuracy in the deconfining phase of SU(2) Yang-Mills thermodynamics. Sec. 3 presents numerical results for the three branches that occur at low momenta. We also present fits to affine power laws of the temperature dependence of characteristic points in the dispersion laws. The energy density of each branch is computed for the high-temperature regime in Sec. 4, and a connection to cosmological magnetic seed fields inducing inside astrophysical structures regular magnetic fields, which were amplified by magneto-hydrodynamical (MHD) dynamos, is made. In Sec. 5 we summarize our results.

2 Computation of dispersion laws for longitudinal modes

This section provides the theoretical background on the physics of longitudinal U(1) modes in the sector of tree-level massless gauge modes in deconfining SU(2) Yang-Mills thermodynamics [10]. Greek (latin) indices refer to spacetime (space) coordinates. All calculations are performed in physical unitary-Coulomb gauge where the former gauge condition relates to a choice of direction in the Lie algebra for the caloron-anticaloron induced, inert and adjoint scalar field ϕ [9]. For definiteness one demands $\phi^a \equiv 2|\phi|\delta^{a3}$ where $|\phi| \equiv \sqrt{\frac{1}{2}\text{tr}\phi^2}$. The Coulomb condition $\partial_i a_i^3 = 0$ requires the modes of the massless, effective gauge field a_μ^3 to be spatially transverse. Given canonical behavior at spatial infinity, this fixes the intact U(1) gauge symmetry physically in a unique way. (The freedom of applying time-dependent U(1) gauge transformations is lost by demanding a_0^3 to decay to zero towards spatial infinity.)

2.1 Preliminaries

Let us briefly review how the calculation of the one-loop dispersions of the longitudinal polarization state of the massless mode proceeds in the effective theory for the deconfining phase [10, 12, 13, 25]. All calculations are performed in unitary-Coulomb gauge. In this physical gauge the formulation of constraints on loop-momenta is simple [11]. As in the transverse case our strategy is to compute in Minkowskian signature the dispersion due to diagram B of Fig. 1 and to subsequently check selfconsistency by demonstrating that diagram A is nil on the so-determined shell $p^2 = F$ where F denotes the longitudinal screening function, see below.

On the one-loop level² the task is the determination of the invariant F in the 00

²In applications (SU(2)_{CMB}) this accuracy is sufficient owing to the fast convergence of the

component of the interacting (imaginary-time) propagator (for an extended discussion see Sec. 3.5.1 of [23])

$$D_{ab,\mu\nu}^{\text{TLM}}(p) = -\delta_{a3}\delta_{b3}\left\{P_{\mu\nu}^T\frac{1}{p^2+G} + \frac{p^2}{\mathbf{p}^2}\frac{1}{p^2+F}u_\mu u_\nu\right\}, \quad (1)$$

where

$$P_{00}^T = P_{0i}^T = P_{i0}^T = 0, \quad (2)$$

$$P_{ij}^T = \delta_{ij} - \frac{p_i p_j}{\mathbf{p}^2}, \quad (3)$$

and $u_\mu = \delta_{\mu 4} = \delta_{\mu 0}$ represents the four-velocity of the heat bath. Due to the intact U(1) gauge symmetry the polarization tensor $\Pi_{\mu\nu}$ of the massless mode is 4D transverse,

$$p_\mu \Pi_{\mu\nu} = 0, \quad (4)$$

and the following decomposition holds

$$\Pi_{\mu\nu} = G(p_4, \mathbf{p}) P_{\mu\nu}^T + F(p_4, \mathbf{p}) P_{\mu\nu}^L, \quad (5)$$

where

$$P_{\mu\nu}^L \equiv \delta_{\mu\nu} - \frac{p_\mu p_\nu}{p^2} - P_{\mu\nu}^T. \quad (6)$$

Obviously, P_{ij}^L is spatially longitudinal and, according to the decomposition in Eq. (5), $\Pi_{44} = F\left(1 - \frac{p_4^2}{p^2}\right)$. In Eq. (5) we suppress the temperature dependences of the invariants G and F arising by a resummation of one- to infinite-fold insertions of $\Pi_{\mu\nu}$ into the free propagator $D_{ab,\mu\nu}^{\text{TLM},0}(p)$ given as

$$D_{ab,\mu\nu}^{\text{TLM},0}(p) = -\delta_{a3}\delta_{b3}\left\{\frac{P_{\mu\nu}^T}{p^2} + \frac{u_\mu u_\nu}{\mathbf{p}^2}\right\}. \quad (7)$$

For Minkowskian signature it was argued in [25] that in both limits $\mathbf{p} \rightarrow 0$ at $p_0 = 0$ and $|p_0| \rightarrow |\mathbf{p}|$ the behavior of function F is not interesting. Namely, we have that $|F| \rightarrow \infty$ in the former and $F \rightarrow 0$ in the latter case. While $|F| \rightarrow \infty$ decouples the longitudinal mode from the spectrum of propagating excitations $F \rightarrow 0$ clashes with the free limit where, according to Eq. (7), the longitudinal mode is instantaneous. (Recall that $|p_0| \rightarrow |\mathbf{p}|$ or $p^2 = 0$ was assumed.) As we will show below, this contradiction is resolved by the selfconsistent determination of the dispersion law: With a cutoff on $|\mathbf{p}|$ the situation $|p_0| \rightarrow |\mathbf{p}|$ takes place as the high-temperature limit in one of three possible branches.

In Fig. 1 the two diagrams, which potentially contribute to $\Pi_{\mu\nu}$, are depicted. In

effective loop expansion [11, 25, 27].

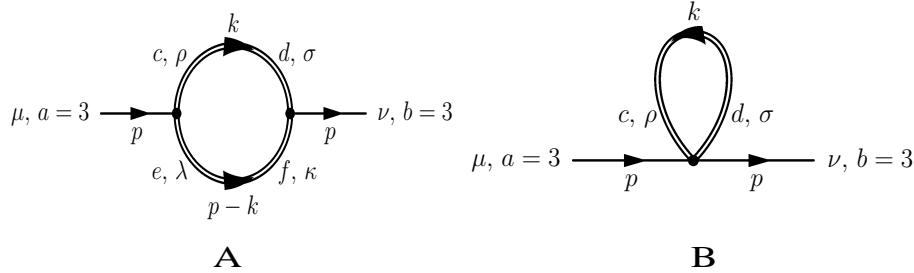


Figure 1: Two one-loop diagrams which potentially contribute to the polarization tensor of the massless mode of deconfining SU(2) Yang-Mills thermodynamics. Single lines are associated with the external ‘photon’ field, double lines depict the propagation of tree-level heavy modes in the thermal loops. (These latter modes occur on their mass-shell only, $k^2 = m^2 = 4e^2|\phi|^2$, where e denotes the effective gauge coupling [10, 12].)

Minkowskian signature restriction to the shell $p^2 = F$ yields [26]

$$\begin{aligned} F(p_4, \mathbf{p}) &= \left(1 - \frac{p_4^2}{p^2}\right)^{-1} \Pi_{44} \rightarrow F(p_0, \mathbf{p}) = -\left(1 - \frac{p_0^2}{p^2}\right)^{-1} \Pi_{00} \Rightarrow \\ \mathbf{p}^2 &= \Pi_{00}. \end{aligned} \quad (8)$$

The right-hand side of the gap equation $\mathbf{p}^2 = \Pi_{00}$ implicitly depends on F through a vertex constraint that must be applied to diagram B in the effective theory [10], and for a given value³ of $|\mathbf{p}|$ the value of F is determined by numerical inversion of the last-line equation in (8). Finally, the propagation of the longitudinal mode is determined by

$$\begin{aligned} \omega^2(\mathbf{p}) &= \mathbf{p}^2 + \text{Re } F(\mathbf{p}), \\ \gamma(\mathbf{p}) &= -\frac{1}{2\omega} \text{Im } F(\mathbf{p}), \end{aligned} \quad (9)$$

where ω and $\gamma^{-1}(\mathbf{p})$ represent energy and lifetime of the longitudinal mode at momentum \mathbf{p} . A finite lifetime or an imaginary contribution to F can, however, only be generated by diagram A (‘photon’ decay into two massive vector modes). However, diagram A turns out to vanish at $p^2 = F$ with F determined by diagram B only, see also [13] for the transverse case.

³Due to the isotropy of the thermal plasma the dependence of Π^{00} on \mathbf{p} is through $|\mathbf{p}|$ only.

2.2 Gap equation

Here we give the equation explicitly that determines the values of F at a given momentum modulus $|\mathbf{p}|$. It is advantageous to express energy ω and $|\mathbf{p}|$ in terms of the dimensionless ratios $X \equiv \frac{|\mathbf{p}|}{T}$ and $Y \equiv \frac{\omega}{T}$ where T denotes temperature. The gap equation $\mathbf{p}^2 = \Pi_{00}$ then is re-cast as

$$X^2 = \frac{\Pi_{00}}{T^2}. \quad (10)$$

Without restriction of generality we may assume that $\mathbf{p} = |\mathbf{p}|e_z$ where e_z is the unit vector in 3-direction. After a change to cylindrical coordinates and a re-scaling of the integration variables the contribution from diagram B of Fig. 1 to the right-hand side of Eq. (10) reads [25]

$$\begin{aligned} X^2 &= \frac{\Pi_{00}}{T^2} \\ &= \int d\xi \int d\rho \, 2e^2 \lambda^{-3} \left(3 + \frac{\rho^2 + \xi^2}{4e^2} \right) \rho \frac{n_B \left(2\pi \lambda^{-3/2} \sqrt{\rho^2 + \xi^2 + 4e^2} \right)}{\sqrt{\rho^2 + \xi^2 + 4e^2}} \quad (11) \end{aligned}$$

$$\equiv \int d\xi \int d\rho \, h_F(\xi, \rho, \lambda), \quad (12)$$

where $n_B(x) \equiv \frac{1}{e^x - 1}$, $\lambda \equiv \frac{2\pi T}{\Lambda}$, and Λ denotes the Yang-Mills scale. The temperature dependence of the effective gauge coupling e is a consequence of thermodynamical consistency of the pressure at the one-loop level, and e exhibits a logarithmic pole at $T_c = \frac{\Lambda}{2\pi} \lambda_c$ ($\lambda_c = 13.89$ refers to the critical temperature of the deconfining-preconfining phase transition [10]) which rapidly relaxes to $e \equiv \sqrt{8}\pi$ as T increases [12]. The right-hand side of Eq. (12) is understood as a sum of two contributions obtained by constraining the integration to the two sets determined by the following conditions (compare with the implementation of the s -channel constraint on the four-vertex in [13])

$$s_{\pm}(\xi, \rho, \lambda, X, f) \leq 1, \quad (13)$$

where

$$s_{\pm}(\xi, \rho, \lambda, X, f) \equiv \left| \frac{f\lambda^3}{(2\pi)^2} + \frac{\lambda^{3/2}}{\pi} \left(\pm \sqrt{X^2 + f} \sqrt{\rho^2 + \xi^2 + 4e^2} - \xi X \right) + 4e^2 \right|, \quad (14)$$

and we have defined $f \equiv \frac{F}{T^2}$. These constraints on the loop integration are a specific manifestation of the general requirement that in the effective four-vertex all three independent 2→2 scattering channels (Mandelstam variables s , t , and u) do not convey momentum transfers larger than the scale $|\phi| \equiv \sqrt{\frac{\Lambda^3}{2\pi T}}$. Recall that this scale emerges from an estimate of the thermal ground state based on BPS

saturated fundamental field configurations [10] which implies that the field ϕ is inert. Because tree-level massive modes propagate on shell [12] the variables t and u satisfy their constraints trivially in our case, and (13) represents the s -channel constraint on positive- and negative-frequency loop four-momenta given an external four-momentum on the shell $Y^2 - X^2 = f$. Taking into account conditions (13), Eq. (12) is re-cast as

$$X^2 - H_F(\lambda, X, f) = 0, \quad (15)$$

where

$$H_F(\lambda, X, f) \equiv \sum_{\sigma=+,-} \int_{-\infty}^{\infty} d\xi \int_0^{\infty} d\rho \theta(1 - s_{\sigma}(\xi, \rho, \lambda, X, f)) h_F(\xi, \rho, \lambda), \quad (16)$$

and $\theta(x)$ denotes the Heaviside step function.

3 Numerical evaluation and characterization

Let us now solve the gap equation (15). Given a value of $\lambda \geq \lambda_c$ and depending on X , Eq. (15) possesses in f no solution at all or up to three solutions. That is, in contrast to the transverse case, where the screening function $g \equiv \frac{G}{T^2}$ is a function of X at a given value of λ , there are three branches in the longitudinal case: f is split into several branches which are separated by isolated singularities of the group velocity $v_g \equiv \frac{d\omega}{d|\mathbf{p}|} = \frac{dY}{dX} = \frac{d\sqrt{X^2+f}}{dX}$. To cope with this situation numerically, we prescribe values for f and λ and search the root of Eq. (15) in variable X . This root turns out to be unique, that is, X is a function of f . In Fig. 2 the three branches of longitudinal dispersion, $Y = \sqrt{X^2+f}$, are plotted for $\lambda = 7.33\lambda_c; 12.82\lambda_c; 18.32\lambda_c$. For $1.83\lambda_c \leq \lambda \leq 20.15\lambda_c$ excellent fits of the λ dependences of X_l and the characteristic points P_1 and P_2 (see Fig. 2) to affine power laws yield

$$\begin{aligned} X_l &= 0.3104 + 0.4853 \left(\frac{\lambda}{\lambda_c}\right)^{-2.987}, & Y_l &= 0.3104 + 0.4971 \left(\frac{\lambda}{\lambda_c}\right)^{-2.991}, \\ P_{1,X} &= -0.0006 + 0.0493 \left(\frac{\lambda}{\lambda_c}\right)^{-0.6798}, & P_{1,Y} &= 0.0013 + 2.348 \left(\frac{\lambda}{\lambda_c}\right)^{-1.533}, \\ P_{2,X} &= 0.0906 + 0.1798 \left(\frac{\lambda}{\lambda_c}\right)^{-3.080}, & P_{2,Y} &= 3.188 - 24.12 \left(\frac{\lambda}{\lambda_c}\right)^{-3.098}. \end{aligned} \quad (17)$$

Notice that the exponents ν in (17) are quite close to simple fractions: $|\nu| \sim 3, \frac{3}{2}, \frac{2}{3}$. In Figs. 3 and 4 plots of X_l , Y_l and $P_{1,X}, P_{1,Y}, P_{2,X}, P_{2,Y}$ together with the fitted curves are shown, respectively. We have checked numerically that besides the pow-

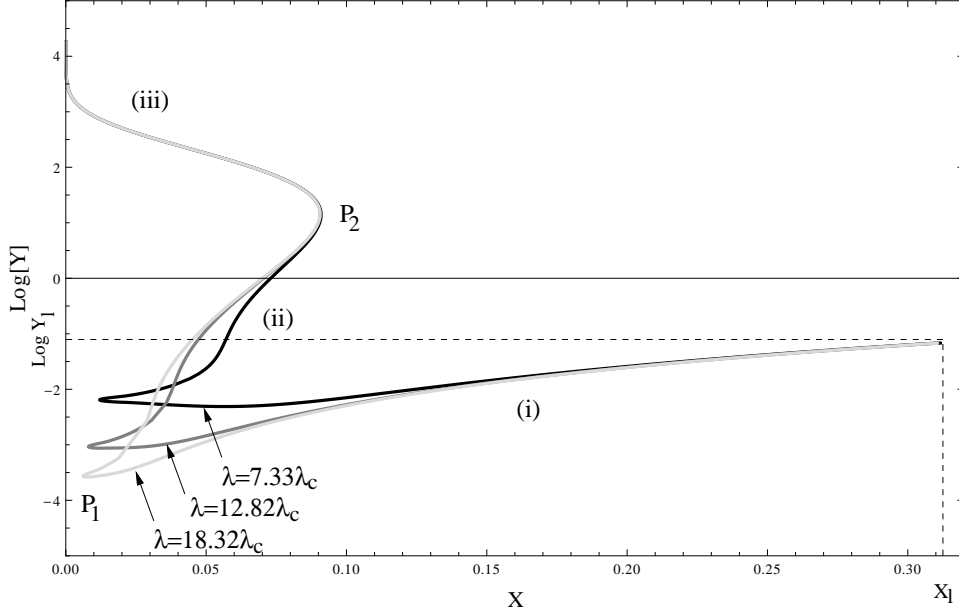


Figure 2: Three branches of the dispersion for longitudinal modes at $\lambda = 7.33 \lambda_c; 12.82 \lambda_c; 18.32 \lambda_c$ where $\lambda_c = 13.87$. The momenta in all three branches (i), (ii), and (iii) are bounded from above by X_l whose high-temperature limit is given as $\lim_{\lambda \rightarrow \infty} X_l = 0.3104 = \lim_{\lambda \rightarrow \infty} Y_l$. The high-temperature limit of the first point P_1 , where the group velocity v_g becomes singular, $|v_g| \rightarrow \infty$, is $\lim_{\lambda \rightarrow \infty} P_{1,X} = \lim_{\lambda \rightarrow \infty} P_{1,Y} = 0$. Branch (i), which is supported by $P_{1,X} \leq X \leq X_l$, approaches a photonlike dispersion law $Y = X$ as $\lambda \rightarrow \infty$. For P_2 one has $\lim_{\lambda \rightarrow \infty} P_{2,X} = 0.0906$; $\lim_{\lambda \rightarrow \infty} P_{2,Y} = 3.188$. Branch (ii), which is supported by $P_{1,X} \leq X \leq P_{2,X}$, exhibits superluminal group velocity, $v_g > 1$. Branch (iii), which is supported by $0 \leq X \leq P_{2,X}$, exhibits negative group velocity of superluminal modulus.

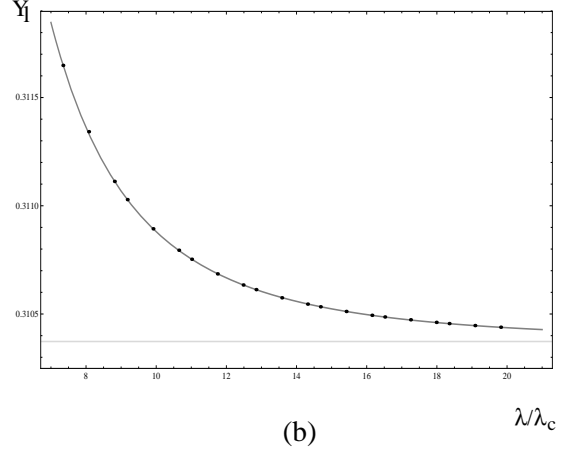
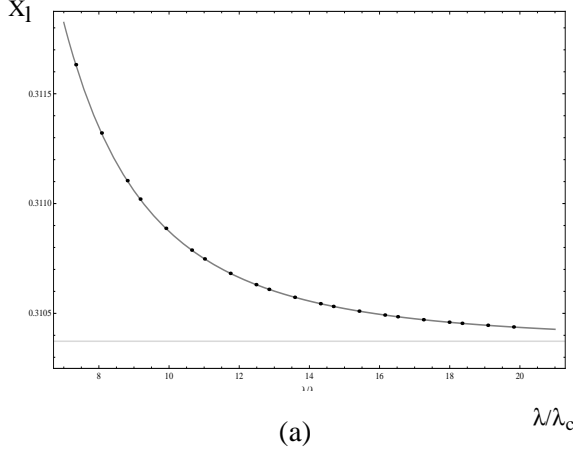


Figure 3: Plots of the λ dependences: (a) X_l and (b) Y_l . Dots are the results of the computation based on Eq. (15), and solid lines represent the affine-power-law fits of Eq. (17).

erlike saturation of X_l and $P_{1,X}, P_{1,Y}, P_{2,X}, P_{2,Y}$, all intermediate sections of the curves in Fig. 2 saturate rapidly to their limit shapes as $\lambda \rightarrow \infty$. Finally, we have checked that on branches (i), (ii), and (iii) the contribution of diagram A in Fig. 1 to Π_{00} vanishes identically.

Let us now attempt a microscopic interpretation of branches (i), (ii), and (iii). The modes in branch (i) are essentially propagating at the speed of light, and it is conceivable that the associated fluctuations in the macroscopic electric charge density are induced by the slow collective motion of stable magnetic (anti)monopoles [24]: Microscopically, the acceleration of a given monopole influences the state of motion of adjacent monopoles through a radiation field which propagates at the speed of light, and no other spatially correlating mechanism exists. This is because a given, stable monopole owes its life to the *dissociation*, that is, destruction of a large-holonomy (anti)caloron whose services in mediating instantaneous spatial correlations from monopole to antimonopole are thus not available. On the other hand, the superluminal propagation of radiatively induced electric charge density in branches (ii) and (iii) with its larger frequencies Y at given value of X should have a microscopic explanation in terms of the instantaneously correlated motion of a short-lived monopole and its antimonopole inside a small-holonomy (anti)caloron.

For isotropic and homogeneous thermalization the superluminal nature of branches (ii) and (iii) does not contradict Special Relativity. This is because the longitudinal modes of $SU(2)_{\text{CMB}}$ are, due to a electric-magnetically dual interpretation, propagating *magnetic* fields of large wavelength⁴ which do not deposit energy in a detector. As a consequence, it is impossible to employ these modes for signal transduction.

4 High-temperature behavior of energy density

Here we discuss the high-temperature behavior of the contributions of branches (i), (ii), and (iii) to the total thermal energy density ρ_L of propagating longitudinal modes. Moreover, we discuss the role of branch (i), which dominates ρ_L , in potentially providing magnetic seed fields for MHD dynamos upon the breaking of spatial isotropy and homogeneity by astrophysically and large-scale structured matter.

4.1 Analytical expressions and numerical results

In the effective theory for deconfining $SU(2)$ Yang-Mills thermodynamics [10] longitudinal modes of the tree-level massless sector are absent on tree level. They emerge as thermal quasiparticles by a resummation of the 00 component of the one-loop polarization tensor. For the energy density ρ_L of longitudinal quasiparticles we

⁴For example, $X_l \sim 0.31$ and $T = 30\text{ K}$; 3000 K imply a minimal wavelength of about 1.6 mm ; $16\mu\text{m}$.

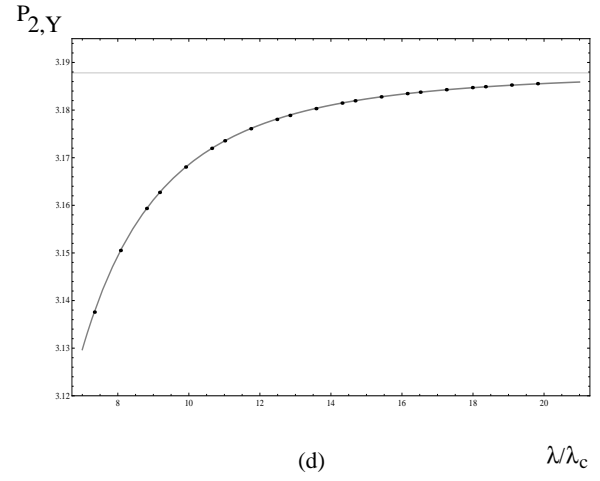
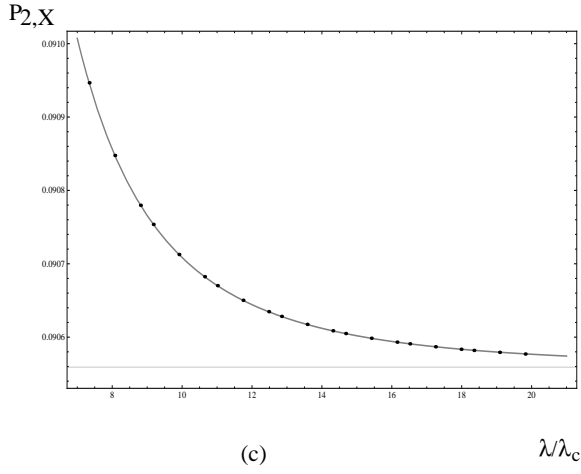
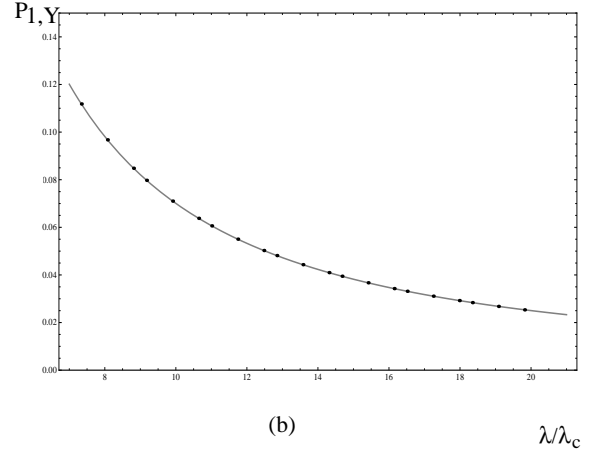
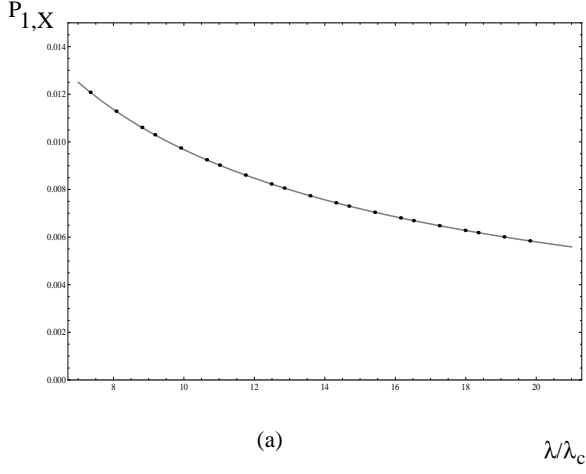


Figure 4: Plots of the λ dependences: (a) $P_{1,X}$, (b) $P_{1,Y}$, (c) $P_{2,X}$, and (d) $P_{2,Y}$. Dots are the results of the computation based on Eq. (15), and solid lines represent the affine-power-law fits of Eq. (17).

have

$$\begin{aligned}
\rho_L(\lambda) &= \rho_{L,(i)}(\lambda) + \rho_{L,(ii)}(\lambda) + \rho_{L,(iii)}(\lambda) \\
&= \frac{T^4}{2\pi^2} \sum_{B=(i),(ii),(iii)} \int_0^\infty dX X^2 \\
&\quad \times \theta(X - X_{B,\min}) \theta(X_{B,\max} - X) \frac{Y_B(X)}{\exp(Y_B(X)) - 1}, \tag{18}
\end{aligned}$$

where

$$\begin{aligned}
X_{(i),\min} &\equiv P_{1,X} \equiv X_{(ii),\min}, & X_{(i),\max} &\equiv X_l, \\
X_{(ii),\max} &\equiv P_{2,X} \equiv X_{(iii),\max}, & X_{(iii),\min} &\equiv 0, \tag{19}
\end{aligned}$$

and $Y_B(X)$ refers to the dispersion law in branch $B = (i),(ii),(iii)$. We have seen in Sec. 3 that there is a rapid saturation of the curves in Fig. 2 to their limit shapes as $\lambda \rightarrow \infty$. By virtue of Eq. (18) this implies that $\frac{\rho_{L,B}(\lambda)}{T^4}$ approach constants at high temperature. One has

$$\begin{aligned}
\lim_{\lambda \rightarrow \infty} \frac{\rho_{L,(i)}(\lambda)}{T^4} &= 4.49 \times 10^{-4}, & \lim_{\lambda \rightarrow \infty} \frac{\rho_{L,(ii)}(\lambda)}{T^4} &= 7.3 \times 10^{-6} \\
\lim_{\lambda \rightarrow \infty} \frac{\rho_{L,(iii)}(\lambda)}{T^4} &= 2.37 \times 10^{-7}, & \lim_{\lambda \rightarrow \infty} \frac{\rho_L(\lambda)}{T^4} &= 4.57 \times 10^{-4}. \tag{20}
\end{aligned}$$

Thus, compared to the Stefan-Boltzmann law $\rho_T = \frac{\pi^2}{15} T^4 \sim \frac{2}{3} T^4$ for two species of transverse, massless photons, the correction ρ_L is about a tenth of a per mille for $\lambda \gg \lambda_c$. Recall from Sec. 3 that the presence of this energy density in $SU(2)_{\text{CMB}}$ is not measurable radiometrically.

4.2 Breaking of isotropy and homogeneity: Magnetic seed fields for galactic MHD dynamos?

Let us now, on a rather qualitative and speculative level, discuss the potential role of longitudinal modes on seeding the generation of magnetic fields in astrophysical structures through the MHD dynamo mechanism. According to [28] and references therein the typical strengths of regular magnetic fields are: 2-10 μG inside spiral galaxies including the Milky Way with coherence-length scales comparable to the scale of the galaxies⁵, several μG in elliptical galaxies with coherence-length scales much smaller than those of the spiral galaxies, and 0.1-1 μG in galaxy clusters. Finally, from measurements of the small-angle CMB anisotropy spectrum a limit of $\sim 10^{-8} \text{ G}$ applies to magnetic fields on the present Hubble scale.

For homogeneous thermalization no regular magnetic field is provided by the longitudinal modes of $SU(2)_{\text{CMB}}$ since the plasma is isotropic. (The incoherent contributions of all longitudinal modes cancel.) This situation changes upon the introduction of anisotropies, e.g. by inhomogeneous thermalization. On one hand, the

⁵Exceptions range up to 50 μG and are correlated with extraordinarily high star-formation rates.

associated temperature gradient would introduce a gradient to the mass of the tree-level massive modes leading to a direction dependence of Π_{00} and F and thus to the emergence of a nonvanishing magnetic field, compare with Fig. 1. This field could then seed MHD dynamos in astrophysical structures. On the other hand, temperature gradients induce a thermoelectric effect by virtue of the ground-state physics of $SU(2)_{\text{CMB}}$ [23] which could amplify the MHD dynamo mechanism by additional current density.

For an upper bound on the field strength expected from longitudinal modes upon the breaking of isotropy and homogeneity in the $SU(2)_{\text{CMB}}$ plasma we compute

$$\bar{B} \equiv \sqrt{\langle \mathbf{B}^2 \rangle_{\text{th}}} = \sqrt{2\rho_L} = T_c^2 \left(\frac{T}{T_c} \right)^2 \sqrt{2 \times 4.57 \times 10^{-4}}. \quad (21)$$

Eq. (21) represents an upper bound because it assumes that the entire energy density of the incoherent longitudinal B -field modes is, by an external cause, converted into the energy density of a coherent B -field. Recall that $T_c = 2.73$ K for $SU(2)_{\text{CMB}}$. Use of $1 \text{ K} = 0.862 \times 10^{-4} \text{ eV}$ and $1 \text{ eV}^2 = 14.4 \text{ G}$ yields

$$\bar{B} = 2.41 \times 10^{-8} \left(\frac{T}{T_c} \right)^2 \text{ G}. \quad (22)$$

That is, the value of \bar{B} scaled to the present epoch ($T = T_c$) via Eq. (22) is about $\sim 10^{-8} \text{ G}$. Thus the order of magnitude of \bar{B} coincides with the upper bound on Hubble-scale, present-day field strength derived from small-angle CMB anisotropies [28], see above.

5 Summary

To summarize, we have computed the dispersion of longitudinal $U(1)$ modes in a selfconsistent way at one-loop accuracy in the effective theory for the deconfining phase of $SU(2)$ Yang-Mills thermodynamics. These modes do not occur on tree level and represent the propagation of radiatively induced electric charge density (charge-density waves). We have characterized the three branches of longitudinally propagating electric fields which occur at low momenta. Two branches are superluminal. We have discussed why superluminal group velocities do not contradict Special Relativity. Namely, the associated long-wavelength and high-frequency modes represent thermalized, propagating *magnetic* fields upon an electric-magnetically dual interpretation of $SU(2)_{\text{CMB}}$ [10, 15]. Due to their incoherent nature and their long wavelengths these modes do not deposit energy in a detector and thus can not be employed for signal transduction. As a next step, we have in the high-temperature regime computed the energy densities associated with each branch. Their sum represents a correction on the tenth-of-a-per-mille level to the Stefan-Boltzmann law for the two polarization states of the massless photon. Finally, we have speculated

upon the role played by the longitudinal $U(1)$ sector of deconfining $SU(2)_{\text{CMB}}$ for the seeding of MHD dynamos to generate the presently observed magnetic fields inside astrophysical structures [28]. Coherent seed fields can only emerge upon a breakdown of spatial isotropy and homogeneity in the plasma leading to a temperature gradient. Driven by gravitational interaction such a gradient is provided naturally by those structures. Taking the thermal energy density inherent to the longitudinal, magnetic $U(1)$ sector of $SU(2)_{\text{CMB}}$ as an upper bound for coherent field energy, we derive an upper bound for the cosmological present-day field strength of about 10^{-8} Gauss. The order of magnitude of this bound coincides with the one obtained from an analysis of CMB small-angle anisotropies, see [28] and references therein.

References

- [1] G. 't Hooft and M. Veltman, Nucl. Phys. B **44**, 189 (1972).
G. 't Hooft and M. Veltman, Nucl. Phys. B **50**, 318 (1972).
G. 't Hooft, Nucl. Phys. B **33**, 173 (1971).
- [2] B. W. Lee and J. Zinn-Justin, Phys. Rev. D **5**, 3121 (1972).
- [3] B. J. Harrington and H. K. Shepard, Phys. Rev. D **17**, 2122 (1977).
- [4] W. Nahm, Phys. Lett. B **90**, 413 (1980).
W. Nahm, CERN preprint TH-3172 (1981).
W. Nahm in *Monopoles in Quantum Field Theory*, ed. N. Craigie *et al.* (World Scientific, Singapore) (1982).
W. Nahm in *Trieste Group Theor. Method 1983* (1983).
W. Nahm in *The ADHM construction for instantons, self-dual monopoles and calorons*, Lect. Notes in Physics Vol. 201, eds. G. Denaro (Springer Heidelberg) (1984).
- [5] D. J. Gross, R. D. Pisarski, and L. G. Yaffe, Rev. Mod. Phys. **53**, 43 (1981).
- [6] K.-M. Lee and C.-H. Lu, Phys. Rev. D **58**, 025011 (1998).
- [7] T. C. Kraan and P. van Baal, Nucl. Phys. B **533**, 627 (1998).
T. C. Kraan and P. van Baal, Phys. Lett. B **435**, 389 (1998).
- [8] D. Diakonov et al., Phys. Rev. D **70**, 036003, (2004).
- [9] U. Herbst and R. Hofmann, arXiv:hep-th/0411214v4 (2004).
- [10] R. Hofmann, Int. J. Mod. Phys. A **20**, 4123 (2005); Erratum-ibid. A **21**, 6515 (2006).
- [11] R. Hofmann, arXiv:hep-th/0609033v4 (2006).

- [12] R. Hofmann, arXiv:0710.0962v3 (2007).
- [13] J. Ludescher and R. Hofmann, *Annalen Phys.* **18**, 271 (2009).
- [14] C. Falquez, R. Hofmann, and T. Baumbach, *Annalen Phys.* **522**, 904 (2010).
- [15] F. Giacosa and R. Hofmann, *Eur. Phys. J. C* **50**, 635 (2007).
- [16] D. J. Fixsen et al., arXiv:0901.0555 (2009).
- [17] C. J. Copi et al., *Adv. Astron.* **2010** 847541 (2010).
M. Tegmark, A. de Oliveira-Costa, and A. J. S. Hamilton, *Phys. Rev. D* **68**, 123523 (2003).
A. de Oliveira-Costa, *Phys. Rev. D* **69**, 063516 (2004).
C. J. Copi, D. Huterer, and G. D. Starkman, *Phys. Rev. D* **70**, 043515 (2004).
- [18] M. Szopa and R. Hofmann, *JCAP* **03**, 001 (2008).
J. Ludescher and R. Hofmann, arXiv:0902.3898 (2009).
- [19] R. Hofmann, *Annalen Phys.* **18**, 634 (2009).
- [20] P. Sikivie, *Phys. Rev. Lett.* **48**, 1156 (1982).
- [21] J. Preskill, M. B. Wise, and F. Wilczek, *Phys. Lett B* **120**, 127 (1983).
- [22] J. A. Frieman, C. T. Hill, A. Stebbins, I. Waga, *Phys. Rev. Lett.* **75**, 2077 (1995).
- [23] C. Falquez, arXiv:1104.0616 (2011).
- [24] J. Ludescher et al., *Annalen Phys.* **19**, 102 (2009).
- [25] M. Schwarz, R. Hofmann, and F. Giacosa, *Int. J. Mod. Phys. A* **22**, 1213 (2007).
(arXiv:hep-th/0603078)
- [26] J. Kapusta and C. Gale, *Finite-temperature Field Theory: Principles and Applications*, Cambridge monographs on mechanics and applied mathematics, Cambridge University Press (2006).
- [27] D. Kaviani and R. Hofmann, *Mod. Phys. Lett. A* **22**, 2343 (2007).
- [28] L. M. Widrow, *Rev. Mod. Phys.* **74**, 775 (2002).